Si-H bond dynamics in hydrogenated amorphous silicon

R. Jason Scharff and Shawn D. McGrane
Dynamic and Energetic Materials Division, Los Alamos National Laboratory, Los Alamos, New Mexico 87545, USA
(Received 29 March 2007; revised manuscript received 23 May 2007; published 1 August 2007)

The ultrafast structural dynamics of the Si-H bond in the rigid solvent environment of an amorphous silicon thin film is investigated using two-dimensional infrared four-wave mixing techniques. The two-dimensional infrared (2DIR) vibrational correlation spectrum resolves the homogeneous line shapes (<2.5 cm^{-1} linewidth) of the $0\rightarrow1$ and $1\rightarrow2$ vibrational transitions within the extensively inhomogeneously broadened (78 cm^{-1} linewidth) Si-H vibrational band. There is no spectral diffusion evident in correlation spectra obtained at 0.2, 1, and 4 ps waiting times. The Si-H stretching mode anharmonic shift is determined to be 84 cm^{-1} and decreases slightly with vibrational frequency. The $1\rightarrow2$ linewidth increases with vibrational frequency. Frequency dependent vibrational population times measured by transient grating spectroscopy are also reported. The narrow homogeneous line shape, large inhomogeneous broadening, and lack of spectral diffusion reported here present the ideal backdrop for using a 2DIR probe following electronic pumping to measure the transient structural dynamics implicated in the Staebler-Wronski degradation [Appl. Phys. Lett. **31**, 292 (1977)] in *a*-Si:H based solar cells.

DOI: 10.1103/PhysRevB.76.054301 PACS number(s): 42.50.Md

I. INTRODUCTION

Silicon is the most commonly used material in photo- and electroactive materials, and the current commercial photovoltaic (PV) market place is dominated by silicon-based technology.[1–8] High quality single-crystalline silicon (*c*-Si) PV cells generally provide the best performance, while hydrogenated amorphous silicon (*a*-Si:H) thin-film PV cells exhibit low performance.[9] The cost associated with device fabrication is reduced substantially by utilizing thin-film growth methods with inexpensive substrate materials, which have been developed for *a*-Si:H.[10] The low optical absorption in the visible spectrum of *c*-Si requires large thicknesses (~100 μm) of Si in PV cells, while the higher absorption coefficient of *a*-Si:H enables the use of submicron films.[8] Although *c*-Si modules continue to be the dominant product in the market place, "amorphous silicon modules appear to be the ideal future candidate for those PV applications in which low cost is more important than high efficiency."[5]

The principal challenge to the improvement of performance and stability of *a*-Si:H PV cells relates to the light-induced degradation that substantially reduces the efficiency of the device. The photoexcited structural dynamics associated with this phenomenon, known as the Staebler-Wronski effect (SWE), produces defects in the material that ultimately lead to a reduced, yet stabilized electrical conductivity.[11] While the exact mechanism responsible for the photoinduced degradation has yet to be determined experimentally, the prevailing model proposes the creation of metastable defect states that act as additional charge recombination centers, thus reducing efficiency.[12,13] In spite of vigorous research effort and device fabrication advancements, the SWE remains intrinsic to *a*-Si:H films. Until a fundamental understanding of the transient Si-H bond dynamics in *a*-Si:H is achieved, additional technological improvements in performance and stability may remain elusive.

Time-resolved ultrafast infrared experiments using intense picosecond pulses from a free electron laser (FEL) have been carried out previously to study the Si-H (Refs. 14–16) and Si-D (Ref. 17) bond dynamics in *a*-Si films. A universal scaled nonexponential line shape for the $0\rightarrow1$ Si-H vibrational stretch population decay was observed in one-dimensional (1D) transient grating experiments over a wide temperature range. On the other hand, a single exponential decay was found for the pure dephasing time of the $0\rightarrow1$ Si-H vibrational transition. Based on those results, it was determined that the Si-H vibrational mode relaxation proceeded by decaying into three Si-H bending modes and one TA phonon.[14–16] Different behavior was observed for Si-D vibrational relaxation. The Si-D population was found to decay directly into the collective modes of the *a*-Si lattice without exciting a local Si-D bending mode.[17] Studies on *a*-Si:D based *p-i-n* solar cells demonstrated superior stability against hot-electron and photoinduced degradation processes.[18,19] The authors concluded that differences in the photoinduced degradation stabilities of *a*-Si:H and *a*-Si:D were related to the differences in the Si-H and Si-D vibrational dynamics and the ability of the Si-D mode to decay directly into low frequency Si-Si lattice modes very rapidly.[18,19] It was further suggested that since the Si-H stretch does not equilibrate rapidly with the lattice, vibrational energy becomes trapped on the Si-H bond, thereby increasing the dissociation probability of the bond.[18,19] It is clear that direct observation of the photoexcited transient structural dynamics of the Si-H bond would prove extremely useful in understanding photodegradation in *a*-Si:H.

Recent advances in multidimensional Fourier transform spectroscopy have made it possible to probe both electronic and vibrational dynamics of complex molecular systems where transient structural fluctuations are relevant.[20–46] Two-dimensional infrared (2DIR) spectroscopy is a type of coherent multidimensional vibrational spectroscopy capable of observing structural dynamics on subpicosecond time scales, offering numerous advantages over traditional linear or 1D techniques. By analogy to 2D NMR, spectral features are separated along two frequency axes for increased resolution, with off-diagonal cross peaks in the 2DIR spectrum indicat-

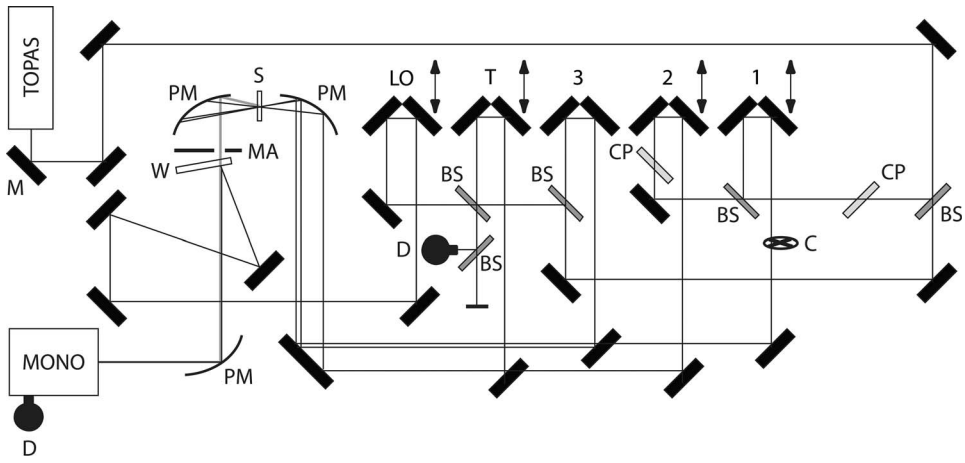

FIG. 1. A schematic of the experimental setup. The five-beam interferometer is composed of the three input pulses (1, 2, and 3), the tracer pulse (T), and the local oscillator pulse (LO). The remaining optical components are denoted as follows: TOPAS, optical parametric amplifier; M, mirror; PM, parabolic mirror; BS, AR-coated Ge beam splitters; CP, compensator plates; C, chopper; S, sample; MA, mask; W, BaF2 window; MONO, monochromator; and D, single-channel HgCdTe detector.

ing coupling between vibrational modes in a variety of local chemical or bonding environments. Because 2DIR includes a rephasing photon echo component, homogeneous linewidths become resolved within an inhomogeneously broadened ensemble. Time-dependent spectral relaxation or diffusion indicative of transient molecular structures, conformational or structural changes, solvent-solute interactions, and vibrational dynamics can be observed by the influence of a second "waiting time" variable in the photon echo pulse sequence. Additionally, intramode and intermode anharmonicities are directly measured for coupled vibrational modes that are excited within the bandwidth of the excitation pulse. As such, 2DIR is an ideal method for probing bond dynamics and degradation mechanisms in semiconductor PV materials such as *a*-Si:H.

In this paper, we present 2DIR vibrational spectra of the Si-H stretching mode in a thin film of *a*-Si:H. The vibrational population dynamics and coherence lifetime of the Si-H bond in the rigid, glassy environment of *a*-Si are investigated using 2D photon echo, 2D transient grating, and degenerate pump-probe absorption methods with mid-infrared femtosecond laser pulses. Using these methods, the frequency dependence is determined for the vibrational anharmonic shift, population lifetime, and coherence dephasing.

II. EXPERIMENTAL METHODS

The experimental details of the interferometer have been described elsewhere.[47] The experimental layout, adapted from Ref. 48, is illustrated in Fig. 1. Briefly, mid-infrared transform-limited, 90 fs pulses centered at 5 μm with $\sim$5 μJ of energy were created by difference frequency generation following optical parametric amplification. The optical parametric amplifier was pumped at 1 kHz with 1 mJ, 45 fs Ti-:sapphire pulses. Each mid-infrared pulse was split into five pulses of approximately 25%/25%/25%/12.5%/12.5% energies along equivalent length paths. Four pulses $\sim$8 mm in diameter ($1/e^2$) were arranged collinearly into a box geometry, focused onto the sample, and collimated after the sample, with 4 in. focal length, 2 in. diameter, 90° off-axis paraboloid reflectors. Three pulses are used for excitation of the four-wave mixing (FWM) signal, and the fourth attenuated (tracer) pulse is made collinear with the FWM signal and used for timing and pump-probe absorption experiments. The tracer is blocked during the rephasing and nonrephasing photon echo experiments. A local oscillator (LO) pulse is made collinear with the FWM signal and combined with the signal. A mask is placed before the spectrometer to isolate the pulse(s) of interest. A large nonresonant signal was observed, substantial even with only two excitation pulses present. This signal was made negligible, while retaining most of the four-wave mixing signal by limiting the total infrared intensity at the sample. A similar but larger spurious signal was observed in 230 μm thick wafers of crystalline Si.

Relative delays were determined with second harmonic generation between pairs of pulses in a $AgGaS_2$ crystal located at the position of the sample. Self-diffraction transient grating geometry frequency resolved optical gating was used to verify optimal compression of the pulses achieved by insertion of dispersion compensating material into the common beam path.

Motorized actuators (Newport LTA) controlled temporal delays that were calibrated at every time step for the rephasing spectral acquisition using a helium-neon laser based Michelson interferometer attached to each delay stage. The nonrephasing spectra reported here have decay times $<$100 fs, and the stage motion was not independently calibrated over this very limited range and resolution. Due to the massive inhomogeneous broadening, the nonrephasing spectra contribute less that 2% to the correlation spectra. Aliased spectra were acquired with time steps of 20 fs. The total time scanned was 3.2 ps to enable resolution of spectral fringes with a 5 nm monochromator step size.

The amorphous silicon sample used in these experiments was grown by plasma-enhanced chemical vapor deposition.

A 1.3 μm thick amorphous film was deposited on a 700 μm thick sapphire substrate, which was polished on both sides. The film thickness was determined from the fringe frequency obtained from broadband Fourier transform infrared (FTIR) absorption. All 2D experiments were performed at room temperature (297 K) with the infrared excitation spectrum centered at 1980 cm^{-1} (5.05 μm) in the ZZZZ (parallel) polarization geometry.

For each waiting time T, rephasing and nonrephasing photon echo signals were acquired using heterodyne-detection based spectral interferometry. Transient grating and pump-probe measurements were acquired without the LO present. For all experiments, the $\boldsymbol{E}_1$ field was mechanically chopped. A boxcar integrator (Stanford Research SR250) used for the single-channel mercury cadmium telluride infrared detector (Infrared Associates) subtracted out the nonchopped signal. The signal was further normalized to a second detector to remove effects of infrared pulse energy fluctuations. The pump-probe experiments utilized the $\boldsymbol{E}_1$ pulse as the pump field and the tracer pulse as the probe field. A lock-in amplifier (Stanford Research SR510) was used for differential detection of the spectrally dispersed probe pulse. To remove residual scattered light contributions that heterodyne the pump-probe signal, the probe delay was dithered over approximately one wavelength by a piezoelectric actuator at $>$200 Hz.

The data were analyzed by Fourier filtering the spectral interferograms at each time step to remove any undesired low frequency components. In practice, this was only required for the nonrephasing echo where the signal was much weaker than the rephasing echo and decayed very quickly. For rephasing and nonrephasing measurements, the spectrally dispersed time data, $\boldsymbol{S}(\boldsymbol{k}_s, \omega_t, T, \tau)$, were interpolated onto evenly spaced frequency and time grids. No temporal filtering or apodization was employed, but the signal decayed substantially by the final time of 3.2 ps after the third pulse. The data are zero padded to a length of 2^{10} and then Fourier cosine transformed to produce the 2D spectrum, $\boldsymbol{S}(\boldsymbol{k}_s, \omega_t, T, \omega_\tau)$. Because the absolute zero timing is not adequately determined, phase error is introduced in the detected signal that must be taken into account. Spectrally dispersed pump-probe signals acquired at each waiting time were used to provide final phasing by projection of the 2DIR correlation spectrum onto the ω_t axis. This was accomplished with a single timing parameter for each rephasing and nonrephasing spectrum, $\Delta t_{\mathrm{LO/E}}$ (the separation between the local oscillator and the echo), which was determined from the spectral interferogram produced by the tracer and local oscillator fields. The 2DIR vibrational correlation spectrum was "phased" by adding a phase correction factor, $\omega \Delta t_{\mathrm{LO/E}}$, to the measured local oscillator and/or tracer phase prior to Fourier cosine transforming the rephasing and nonrephasing data along τ. The required timing corrections were always $<$10 fs to minimize the difference between the pump-probe and 2DIR correlation projection.

III. THEORY

The 2DIR experiment is a time-resolved FWM technique in which three infrared pulses interact within a sample to generate a nonlinear signal containing information regarding the time-dependent changes in the local bonding environment and coupled vibrational modes. Several reviews of the theoretical and experimental aspects of the technique have been published.[48–52] The three time-ordered ultrafast mid-infrared laser fields, denoted $\boldsymbol{E}_1$, $\boldsymbol{E}_2$, and $\boldsymbol{E}_3$ with wave vectors $\boldsymbol{k}_1$, $\boldsymbol{k}_2$, and $\boldsymbol{k}_3$, interact in the sample and generate a complex nonlinear signal field $\boldsymbol{E}_s$ radiating in the phase-matched direction of $\boldsymbol{k}_s = \mp \boldsymbol{k}_1 \pm \boldsymbol{k}_2 + \boldsymbol{k}_3$, where the upper sign signifies the rephasing echo experiment and the lower sign signifies the nonrephasing echo experiment. The six double-sided Feynman pathways illustrated in Fig. 2 describe the rephasing and nonrephasing photon echo signal amplitudes generated from a single, anharmonic oscillator. Vibrational ladder diagrams for each pathway are also included in Fig. 2. Pathways I and II in the rephasing and nonrephasing diagrams shown in Fig. 2 represent single quantum excitations. Double quantum excitations produced by the overtone state are described by pathway III. The signal field is denoted by the wavy arrow and results from the third-order polarization generated by the three matter-field interactions in the sample.

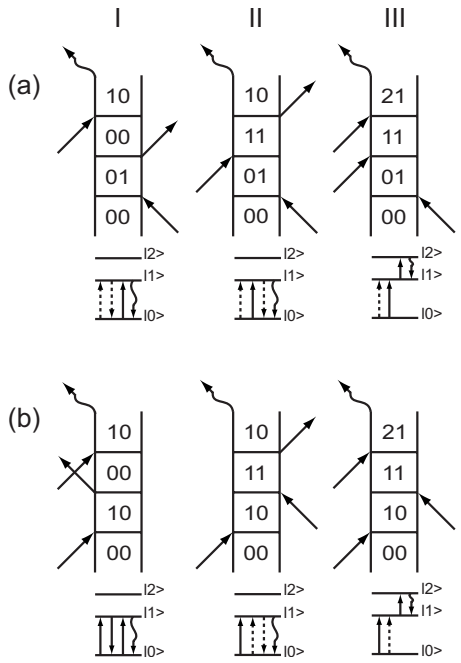

FIG. 2. Double-sided Feynman diagrams and vibrational ladder diagrams corresponding to the (a) rephasing and (b) nonrephasing pathways. Pathways I and II correspond to one-quantum states, while pathway III corresponds to one-quantum and two-quantum states. In the Feynman diagrams, the two vertical lines represent the ket (left) and the bra (right) with time increasing from bottom to top. In the ladder diagrams, solid (dashed) lines correspond to ket (bra) interactions.

The first field applied generates a vibrational coherence within the sample, and after waiting some evolution time τ, the second field interacts with the sample. After a fixed waiting period of T, the third pulse arrives at the sample. The local oscillator field then interferes with the emitted signal, which is detected by spectral interferometry. Spectral interferometric detection produces the same information as the

conceptually simpler method where the local oscillator time gates the signal field radiated at time t.[44]

For a single vibrational mode, the two-dimensional Fourier transform of the real part of the heterodyned radiated signal will have a single peak projected along the ω_τ axis, and will have two peaks projected along the ω_t axis separated by the vibrational anharmonic shift. Rephasing or nonrephasing signals are detected by varying the time orderings of the respective excitation fields at the wave vectors noted above. In the rephasing experiment, the phase acquired by a vibrational coherence during τ is the conjugate of the phase detected at t. In the nonrephasing experiment, the coherences evolve with the same phase during the evolution and detection periods. The vibrational correlation spectrum is the real part of the sum of the rephasing and nonrephasing spectra, resulting in a purely absorptive line shape.[48] In the 2D rephasing and correlation spectra, the inhomogeneous linewidth is observed as an elongated peak along the diagonal axis $\omega_t=\omega_\tau$, whereas the homogeneous linewidth is observed along the antidiagonal. By varying the waiting time T, spectral diffusion may be elucidated if structural fluctuations such as solvent reorganization, bond dissociation, and chemical exchange are present. These structural fluctuations are observed as time-dependent changes the 2DIR spectral features.

In the inhomogeneous limit, line narrowing is only observed in the rephasing photon echo pathway. In notation consistent with Fig. 2, the response functions for the rephasing echo pathways can be expressed as[53]

$$R_{\mathrm{I}} = R_{\mathrm{II}} = \mu_{01}^4 \exp[-i(\omega+\delta\omega)t - \Gamma_{01}t]\exp[i(\omega+\delta\omega)\tau - \Gamma_{01}\tau], \tag{1}$$

$$R_{\mathrm{III}} = \mu_{01}^2\mu_{12}^2 \exp[-i(\omega+\delta\omega-\Delta)t - \Gamma_{01}t - \Gamma_{12}t] \times \exp[i(\omega+\delta\omega)\tau - \Gamma_{01}\tau], \tag{2}$$

such that the ensemble-averaged frequency of the fundamental is given by ω, and $\delta\omega$ is the frequency shift of an individual transition within the ensemble. In general, $\delta\omega$ is used to describe spectral diffusion and would therefore be time dependent. However, it is shown below that the distribution of Si-H oscillators in a-Si is not time dependent, and we therefore take $\delta\omega$ to be static. Furthermore, Δ is the anharmonic shift separating the fundamental and overtone occurring at $2\omega-\Delta$, and Γ_{01} and Γ_{12} describe the motionally narrowed total dephasing rates for the $0\rightarrow1$ and $1\rightarrow2$ transitions.

We treat the excitation pulses in the impulsive limit such that the detected signal is given as[53]

$$S(t,\tau) \propto \mathrm{Re}\{\Re(t,\tau)\}, \tag{3}$$

with

$$\Re(t,\tau) = R_{\mathrm{I}}(t,\tau) + R_{\mathrm{II}}(t,\tau) - R_{\mathrm{III}}(t,\tau). \tag{4}$$

The minus sign in Eq. (4) is due to the odd number of bra interactions in the third pathway as opposed to the even number in the first two pathways.

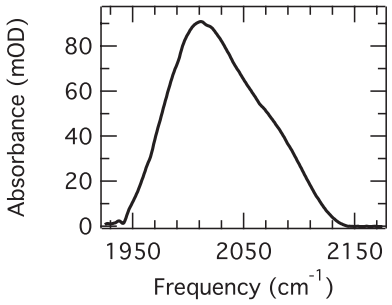

FIG. 3. Infrared absorption spectrum of a-Si:H taken at room temperature. Contributions from isolated Si-H monohydride bonds are peaked at 2010 cm^{-1}. The shoulder apparent on the blue side of the spectrum near 2080 cm^{-1} is attributed to clustered Si-H bonds or SiH_2.

The complex 2D spectrum in the frequency domain is produced by a Fourier-Laplace transformation of Eq. (3) along t and τ to obtain the expression[53]

$$\tilde{S}(\omega_t,\omega_\tau) = \int_0^\infty \int_0^\infty S(t,\tau)e^{-i\omega_t t}e^{-i\omega_\tau \tau}dtd\tau \tag{5}$$

or

$$\tilde{S}(\omega_t,\omega_\tau) = \frac{\mu_{01}^4}{\Gamma_{01}+i(\omega+\delta\omega+\omega_t)} - \frac{\mu_{01}^2\mu_{12}^2}{\Gamma_{01}+\Gamma_{12}+i(\omega+\delta\omega-\Delta+\omega_t)} \Big/ \Gamma_{01}-i(\omega+\delta\omega+\omega_\tau). \tag{6}$$

The effect of inhomogeneous broadening on the spectrum can be included by introducing the normal probability distribution function

$$G(\delta\omega) = \frac{1}{\sigma\sqrt{2\pi}}\exp\left[-\frac{\delta\omega^2}{2\sigma^2}\right], \tag{7}$$

followed by multiplication with Eq. (6) and subsequent integration over $\delta\omega$ such that the complex 2D photon echo signal may be expressed in the following analytic form:

$$S_{PE}(\omega_t,\omega_\tau) = \int_{-\infty}^{\infty} \tilde{S}(\omega_t,\omega_\tau)G(\delta\omega)d\delta\omega. \tag{8}$$

IV. RESULTS

A. Experimental determination of 2DIR spectra

The infrared absorption spectrum of the Si-H stretching mode is shown in Fig. 3. The spectrum is centered at 2010 cm^{-1} and possesses a weak shoulder on the blue side of the band near 2080 cm^{-1}. A sloping base line due to low frequency fringes from multiple reflections has been removed. The extensively inhomogeneously broadened absorption spectrum [105 cm^{-1} full width at half maximum (FWHM)] contains contributions due to the isolated mono-

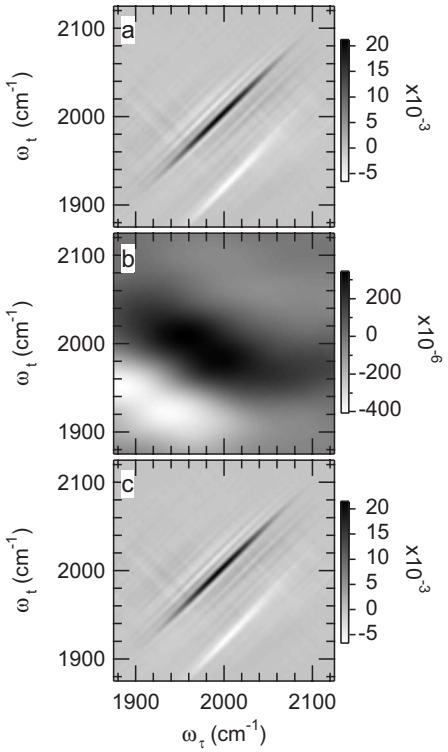

FIG. 4. (a) 2DIR rephasing spectrum, (b) nonrephasing spectrum, and (c) their sum, the correlation spectrum for a-Si:H at $T=1$ ps. Note: the magnitude of the nonrephasing echo is a factor of 60 weaker than the rephasing echo.

hydride bonds (2010 cm^{-1}) and clustered Si-H bonds and/or SiH_2 (2080 cm^{-1}).[54,55]

Figure 4 shows the (a) 2D rephasing echo, (b) nonrephasing echo, and (c) their sum, the correlation spectra for a-Si:H taken at $T=1$ ps. The rephasing and nonrephasing spectra are both characterized by positive and negative features that are elongated along the diagonal (rephasing) and antidiagonal (nonrephasing). Note that we have represented the x axis of the rephasing spectrum to be positive using the convention detailed in Ref. 48. The nonrephasing echo peak magnitude is approximately 60 times weaker than the rephasing echo and consists of very broad and diffuse spectral features. The correlation spectrum shows two elongated spectral features along the diagonal that are oppositely phased. The band along the diagonal with positive intensity is the $0\rightarrow1$ vibrational transition of the Si-H stretch and the band below with negative intensity is the $1\rightarrow2$ vibrational transition. The separation between the $0\rightarrow1$ Si-H vibrational transition and the $1\rightarrow2$ Si-H vibrational transition observed in the correlation spectrum yields the vibrational anharmonic shift.

Small oscillations are apparent and displaced from the $0\rightarrow1$ transition along the ω_τ axis. We have considered the possibility that these artifacts originate from the truncation of data at the end of our scan for the long coherence times of the $0\rightarrow1$ transition. However, we have also acquired 2D echoes for delays up to 12 ps in which the echo has completely decayed, and we have found similar oscillations in the wings of the $0\rightarrow1$ transition. Furthermore, we observe

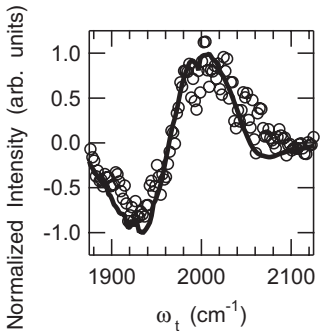

FIG. 5. The ω_t axis projection of the phased 2DIR vibrational correlation spectrum (solid lines) at 1 ps waiting time [Fig. 3(c)] and the spectrally dispersed pump-probe (open circles).

no improvement in the resolution of the homogeneous linewidth. Individual step sizes were calibrated to ~50 nm, which should allow for accurate Fourier transformations. Apodization of the 12 ps data did not decrease the artifacts, suggesting that long-term phase instabilities due to thermally induced pointing changes into the interferometer are not the origin. The most likely remaining origin of the oscillations is multiple reflections intrinsic to the high dielectric constant of the a-Si thin film. Despite the oscillations which are presumably artifact in nature, the $1\rightarrow2$ transition is well resolved under our experimental conditions, while the $0\rightarrow1$ transition is broadened in a consistent manner since all frequencies and waiting times are analyzed with the same total scan time.

The vibrational correlation spectrum in Fig. 4(c) is phased by projecting the correlation spectrum onto the ω_t axis and minimizing the error in the difference between the projection and the dispersed pump-probe spectrum by adjusting the phase correction factor $\omega\Delta t_{\mathrm{LO/E}}$. Figure 5 demonstrates the result of the phasing procedure.

The influence of waiting time T on the 2DIR vibrational correlation spectra is depicted in Fig. 6. Correlation spectra at $T=0.2$, 1, and 4 ps shown in Fig. 6 exhibit no change in the 2DIR spectral features within the resolution of the experiment. Quantitative details determined from the data of Fig. 6 include frequency dependent anharmonicities and linewidths, shown in Fig. 7.

The anharmonic shift decreases slightly, but measurably, as the frequency increases. The anharmonic shift was determined simply from the ω_τ dependent difference between the $0\rightarrow1$ and $1\rightarrow2$ peaks. Linewidths (FWHM) of the $0\rightarrow1$ and $1\rightarrow2$ peaks were determined by fitting the projection onto the ω_t axis to the sum of two displaced Gaussians. While the projection overestimates the linewidth for determination of the decay time due to the convolution between the inhomogeneous and homogeneous distributions, it provides a simple and convenient method of looking for frequency dependent changes. The linewidth of the $0\rightarrow1$ transition is essentially constant and instrumentally limited (note that this is a *projection linewidth* and the absolute magnitude is *not* the homogeneous linewidth). The linewidth of the $1\rightarrow2$ peak is large enough to resolve and demonstrates a slight broadening with increasing frequency.

The spectrally dispersed transient grating, shown in Fig. 8, illustrates Si-H vibrational population relaxation. The

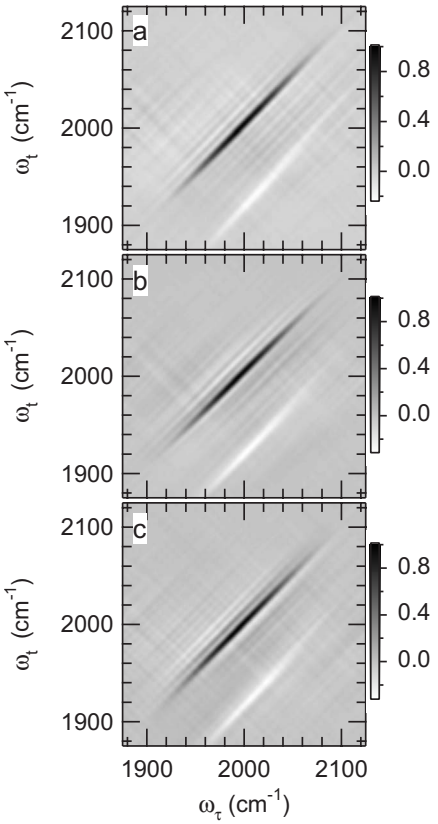

FIG. 6. 2DIR vibrational correlation spectra as a function of waiting time T between the second and third excitation pulses T=(a) 0.2 ps, (b) 1 ps, and (c) 4 ps. Note: the intensity scales have been normalized.

panel on the right provides the excitation spectrum. The intensity of the spectrally dispersed transient grating signal is shown as a function of probe delay where the two pump pulses have been separated by 200 fs. The small time delay between the two pump pulses was necessary to remove a residual zero time delay artifact that causes an anomalous oscillation in the grating decay. The upper panel shows the transient grating signal at 2000 cm^{-1} on a logarithmic intensity scale and demonstrates that the population does not decay with a single exponential time constant. The frequency dependent transient grating decay was fitted to a function that has been empirically found to fit the decay in previous work by Rella *et al.*,[16] the sum of two exponentials squared $I(t) \propto [\exp(-t/\tau_{fast}) + \exp(-t/\tau_{slow})]^2$. The fit through the lineout is purely phenomenological and will be discussed below. The fits describe the data satisfactorily; the parameters determined are shown in Fig. 9.

B. Calculation of the 2DIR spectra

Figure 10(a) provides the fit of the T=1 ps rephasing photon echo experimental data from Fig. 4(a) using the formalism developed in Eqs. (1)–(8). We have used a quasi-Newton nonlinear least squares fitting algorithm to obtain the best-fit parameters. Figure 10(b) gives a lineout from the 2D data (open circles) and calculated spectrum (solid line) taken at

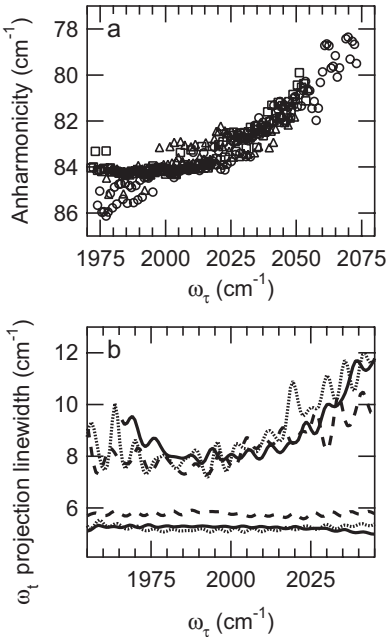

FIG. 7. (a) The frequency dependent anharmonic shift is simply the peak separation for the $0 \rightarrow 1$ and $1 \rightarrow 2$ transitions from the correlation spectra at T=0.2 ps (circles), 1 ps (squares), and 4 ps (triangles). (b) Linewidths of the projection onto the ω_t axis are shown for the $0 \rightarrow 1$ transition (smaller linewidths) and the $1 \rightarrow 2$ transition (larger linewidths) for T=0.2 ps (dashed lines), 1 ps (solid lines), and 4 ps (dotted lines).

ω_τ=−2000 cm^{-1}. An inhomogeneous distribution width of $2\sqrt{2 \ln 2}\sigma$=77.7 cm^{-1} has been assumed in the calculation. It should be noted that this value is smaller than the 105 cm^{-1} FWHM from the linear IR absorption spectrum due to the apparent absence of the SiH_2 shoulder in the 2DIR spectrum and the finite bandwidth of the excitation pulses. In the 2DIR experiment, we are sensitive only to the Si-H distribution. The fit yields homogeneous linewidths for the $0 \rightarrow 1$ and $1 \rightarrow 2$ Si-H transitions of Γ_{01}=1.53 cm^{-1} and

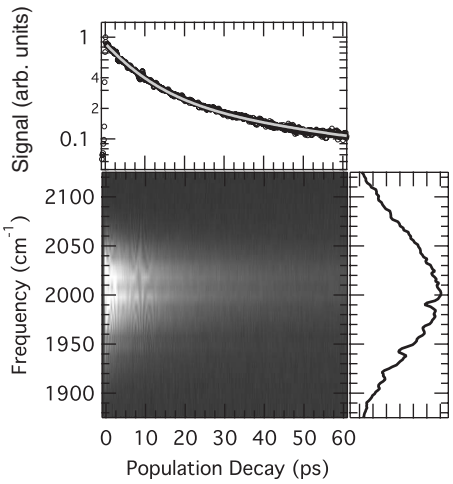

FIG. 8. Spectrally dispersed transient grating decays for the Si-H stretching mode. Top panel: 1D line spectrum taken at 2000 cm^{-1}. Right panel: the excitation spectrum.

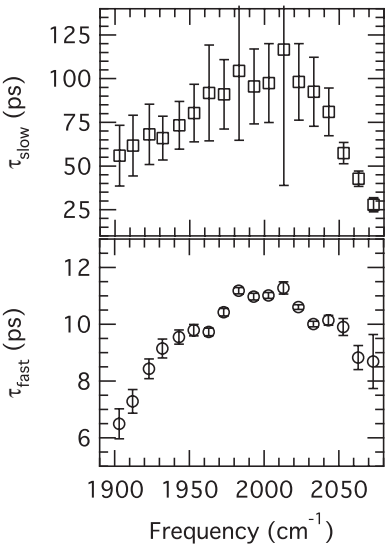

FIG. 9. Frequency dependence for the "fast" and "slow" decay components of the transient grating signal fit to a squared biexponential model (see text for details).

$\Gamma_{12}=2.15\ \mathrm{cm}^{-1}$, respectively. The anharmonic shift at $\omega_\tau=-2000\ \mathrm{cm}^{-1}$ was calculated to be 84.8 cm^{-1}. The ratio of the transition dipoles μ_{01}/μ_{12} was found to be 0.99 compared to $1/\sqrt{2}$ from the harmonic approximation. The frequency dependence of the anharmonicity and $1\rightarrow 2$ transition (projected) linewidths is not included as a part of the photon echo response, and it is therefore unable to be reproduced in the least squares fit of the experimental data.

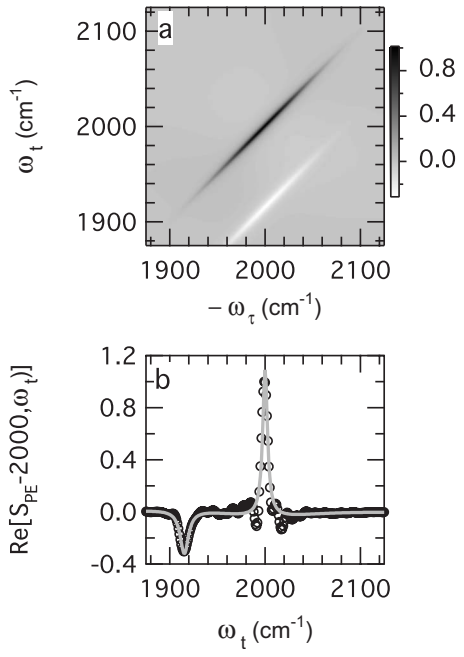

FIG. 10. (a) Calculated 2D rephasing echo spectrum obtained from the nonlinear least squares fit to the experimental data from Fig. 4(b) and (b) the real part of the calculated spectrum (solid line) and experimental lineout (open circles) showing a slice along $\omega_\tau=-2000\ \mathrm{cm}^{-1}$.

V. DISCUSSION

Due to the amorphous nature of the system, the Si-Si lattice may be considered to be a rigid solvent containing randomly oriented Si-H solute molecules in a variety of different local bonding environments, leading to the infrared absorption band observed in Fig. 3. This type of spectrum contains no dynamical information because the system appears static due to the time scale of the experiment, and only represents a time-averaged distribution of molecular states within the ensemble.[52] Fluctuations in the local environment that involve interactions between the Si-H stretch and Si lattice modes further broaden the homogeneous line shape. The FTIR absorption centered at 2080 cm^{-1} is generally interpreted as SiH_2 or clustered Si-H bonds.[54,55] The absorption cross section of the 2080 cm^{-1} band is approximately three times less than the monohydride absorption cross section,[55] and the echo magnitude will square this factor. Nonheterodyned four-wave mixing measurements of the intensity square the dependence on transition dipole moment again for a signal contribution from the SiH_2 or SiH clusters that would be a factor of 81 times less intense than the monohydride species. Also, the Si-H concentration is greatest for the monohydride species. For these reasons, we observe only the monohydride species in the 2DIR spectra shown in Figs. 4 and 6.

In Figs. 4 and 6, the homogeneous linewidth of the $0\rightarrow 1$ transition is more than 50 times less than the massively inhomogeneously broadened ensemble as evidenced in the rephasing and correlation spectra. The nonrephasing spectral features are diffuse and weaker in intensity due to the very fast decay of the nonrephasing echo with the large inhomogeneous bandwidth of *a*-Si:H. In the rigid, glassy network of *a*-Si, the vibrational dephasing time for Si-H bonds is long due to intrinsic constraints on rotational and translational motions resulting in very narrow homogeneous linewidths. The previous photon echo studies determined the average dephasing time to be on the order of 10–15 ps at room temperature, suggesting a homogeneous linewidth of $<1\ \mathrm{cm}^{-1}$ for the $0\rightarrow 1$ transition.[14,15] Based on our fits to the 2D rephasing echo data, the 1.53 cm^{-1} linewidth (resolution is experimentally limited) observed for the $0\rightarrow 1$ transition appears to agree quite well with the FEL results.

In Fig. 6, we find no dependence of the vibrational correlation spectra on waiting time, indicating that structural fluctuations do not occur on the time scale of our experiments. This is not unexpected for a solid material. On the other hand, it is anticipated that spectral diffusion may become evident by optically pumping the material at visible wavelengths. The lack of spectral diffusion is particularly important if this is to be used as an identification mechanism for Staebler-Wronski intermediates[12,13] in transient electronic excitation 2DIR probe in future studies.

The frequency dependence of the anharmonic shift and linewidth of the $1\rightarrow 2$ transition likely originates in the different types of Si-H bonds that occur due to variations in local structure and bonding. There are many different Si-H bond defects that have been resolved and identified in crystalline Si, and corollaries likely exist in *a*-Si:H, but have not been resolved in the large inhomogeneous linewidth. It is not

surprising that different types of Si-H bonds have different frequencies, linewidths, and anharmonicities, but it is also not immediately apparent what this variation will be. The results of Fig. 7 provide these values. Additional experimental and/or computational results are required to definitively assign specific vibrational frequencies to variations in the microscopic nature of the amorphous lattice.

Although we recognize that the transient grating should be composed of a distribution of decays from the $\nu=1$ state, we use the functional form of Rella *et al.*[16] in order to make direct comparisons. In that work, the transient grating signal was acquired for more than 250 ps. Our results focus on the frequency dependence of the "fast" component of the earlier results. The fast component is sensitively determined, whereas the "slow" component less accurately due to the total time scan length of 60 ps. The parameters determined are consistent with previous reports using narrow band FEL pulses. The inhomogeneous distributions of the $0\rightarrow1$ and $1\rightarrow2$ transition frequencies partially overlap and therefore contribute to the observed transient grating decays.

By 3 ps, the echo intensity has decayed by 63%, whereas the population has decayed by only 14%; the echo signal decay is due predominantly to pure dephasing. These results are consistent with the results of van der Voort *et al.*[15] and Rella *et al.*[16] in which pure dephasing was the main contributor to the echo decay. We also find that pure dephasing is largely responsible for the echo decay of the $1\rightarrow2$ transition since the dephasing time is almost a factor of 4 faster than the fast component of the vibrational population relaxation time.

We also speculate on the implications of Si-H bond dynamics coupled with electronic excitation due to visible light pumping. If electron-hole recombination selectively breaks certain Si-H bonds (weak bonds or defects at certain frequencies), a frequency dependent time evolving homogeneous broadening is expected, which can offer detailed insights into transient structures formed. The light-induced degradation of *a*-Si:H associated with the SWE is expected to produce transient structures such as Si dangling bonds and mobile H atoms, which may be observed in transient-2DIR spectra. Electronic pump-2DIR probe difference spectroscopy will be sensitive to small vibrational changes induced by the electronic pump, as appropriate for observation of the light-induced Staebler-Wronski states. The effect of photoexcitation should lead to dephasing times of Si-H shorter than those of stable Si-H bonded species which will be apparent as frequency dependent spectral broadening in the 2DIR rephasing and vibrational correlation spectra. As such, the relevant subset of Si-H bonding environments that contribute to the SWE may be determined by a combination of transient-2DIR spectroscopy with other experimental or theoretical methods.

VI. CONCLUSIONS

Two-dimensional infrared correlation spectra of the Si-H stretching mode in *a*-Si:H were reported for waiting times of 0.2, 1, and 4 ps. The homogeneous linewidth of the $0\rightarrow1$ transition is more than 50 times narrower than the inhomogeneous linewidth, and there is no spectral diffusion observed as a function of waiting time. The anharmonic shift of 84 cm^{-1} is much larger than the homogeneous linewidth (<2.5 cm^{-1}), allowing for the total separation of the $0\rightarrow1$ and $1\rightarrow2$ transitions. The anharmonic shift decreases slightly with frequency. The $0\rightarrow1$ linewidth is constant with Si-H stretch frequency within our instrumental resolution, but the $1\rightarrow2$ linewidth increases with increasing frequency, reflecting the different local structures that correspond to different vibrational frequencies. Transient grating also shows frequency dependent decays. These results offer quantitative measurements of *a*-Si:H vibrational dynamics beyond those accessible with previous methods. In addition, the combination of narrow homogeneous linewidths, broad inhomogeneous linewidths with frequency dependent properties, and lack of spectral diffusion establishes the ideal base line for studies of transient-2DIR probe following an electronic excitation. Transient-2DIR following electronic excitation offers future potential to deduce structural dynamics of the Staebler-Wronski degradation relevant to the photovoltaic performance of *a*-Si:H films.

ACKNOWLEDGMENTS

The authors gratefully acknowledge the support of this work through the Los Alamos National Laboratory Directed Research and Development Exploratory Research program. We also thank J. I. Dijkhuis (Universiteit Utrecht) for providing the *a*-Si:H sample used in this work.

[1] A. V. Shah, H. Schade, M. Vanecek, J. Meier, E. Vallat-Sauvain, N. Wyrsch, U. Kroll, C. Droz, and J. Bailat, Prog. Photovoltaics **12**, 113 (2004).
[2] R. E. I. Schropp, Thin Solid Films **451/452**, 455 (2004).
[3] M. A. Green, Sol. Energy **76**, 3 (2004).
[4] A. Goetzberger, C. Hebling, and H. W. Schock, Mater. Sci. Eng., R. **R40**, 1 (2003).
[5] A. Shah, P. Torres, R. Tscharner, N. Wyrsch, and H. Keppner, Science **285**, 692 (1999).
[6] B. Rech and H. Wagner, Appl. Phys. A: Mater. Sci. Process. **69**, 155 (1999).
[7] R. B. Bergmann, Appl. Phys. A: Mater. Sci. Process. **69**, 187 (1999).
[8] A. V. Shah, R. Platz, and H. Keppner, Sol. Energy Mater. Sol. Cells **38**, 501 (1995).
[9] Report of the Basic Energy Sciences Workshop on Solar Energy Utilization, 18–21 April 2005, http://www.sc.doe.gov/bes/reports/files/SEU_rpt.pdf
[10] A. Shah, J. Meier, A. Buechel, U. Kroll, J. Steinhauser, F. Meillaud, H. Schade, and D. Domine, Thin Solid Films **502**, 292 (2006).
[11] D. L. Staebler and C. R. Wronski, Appl. Phys. Lett. **31**, 292

(1977).
[12] H. M. Branz, Phys. Rev. B **59**, 5498 (1999).
[13] H. M. Branz, Solid State Commun. **105**, 387 (1998).
[14] J. P. R. Wells, E. D. van Hattum, R. E. I. Schropp, P. J. Phillips, A. A. Carder, F. H. P. M. Habraken, and J. I. Dijkhuis, Phys. Status Solidi B **241**, 3474 (2004).
[15] M. van der Voort, C. W. Rella, A. F. G. van der Meer, A. V. Akimov, and J. I. Dijkhuis, J. Non-Cryst. Solids **266/269**, 180 (2000).
[16] C. W. Rella, M. van der Voort, A. V. Akimov, A. F. G. van der Meer, and J. I. Dijkhuis, Appl. Phys. Lett. **75**, 2945 (1999).
[17] Jon-Paul R. Wells, R. E. I. Schropp, L. F. G. van der Meer, and J. I. Dijkhuis, Phys. Rev. Lett. **89**, 125504 (2002).
[18] J. P. R. Wells, R. E. I. Schropp, L. F. G. van der Meer, and J. I. Dijkhuis, Proc. SPIE **5352**, 250 (2004).
[19] G. Munyeme, J. P. R. Wells, L. F. G. van der Meer, J. I. Dijkhuis, W. F. van der Weg, and R. E. I. Schropp, J. Non-Cryst. Solids **338/340**, 291 (2004).
[20] J. R. Zheng, K. Kwak, X. Chen, J. B. Asbury, and M. D. Fayer, J. Am. Chem. Soc. **128**, 2977 (2006).
[21] J. P. Wang, J. X. Chen, and R. M. Hochstrasser, J. Phys. Chem. B **110**, 7545 (2006).
[22] J. Park and R. M. Hochstrasser, Chem. Phys. **323**, 78 (2006).
[23] P. Mukherjee, I. Kass, I. Arkin, and M. T. Zanni, Proc. Natl. Acad. Sci. U.S.A. **103**, 3528 (2006).
[24] J. R. Zheng, K. Kwak, J. Asbury, X. Chen, I. R. Piletic, and M. D. Fayer, Science **309**, 1338 (2005).
[25] H. S. Tan, I. R. Piletic, R. E. Riter, N. E. Levinger, and M. D. Fayer, Phys. Rev. Lett. **94**, 057405 (2005).
[26] Y. S. Kim and R. M. Hochstrasser, Proc. Natl. Acad. Sci. U.S.A. **102**, 11185 (2005).
[27] E. C. Fulmer, F. Ding, and M. T. Zanni, J. Chem. Phys. **122**, 034302 (2005).
[28] C. Fang and R. M. Hochstrasser, J. Phys. Chem. B **109**, 18652 (2005).
[29] J. C. Wright, Vib. Spectrosc. **36**, 179 (2004).
[30] J. Park, J. H. Ha, and R. M. Hochstrasser, J. Chem. Phys. **121**, 7281 (2004).
[31] M. Khalil, N. Demirdoven, and A. Tokmakoff, J. Chem. Phys. **121**, 362 (2004).
[32] I. J. Finkelstein, B. L. McClain, and M. D. Fayer, J. Chem. Phys. **121**, 877 (2004).
[33] C. Fang, J. Wang, Y. S. Kim, A. K. Charnley, W. Barber-Armstrong, A. B. Smith, S. M. Decatur, and R. M. Hochstrasser, J. Phys. Chem. B **108**, 10415 (2004).
[34] D. M. Besemann, K. A. Meyer, and J. C. Wright, J. Phys. Chem. B **108**, 10493 (2004).
[35] J. B. Asbury, T. Steinel, C. Stromberg, K. J. Gaffney, I. R. Piletic, A. Goun, and M. D. Fayer, Phys. Rev. Lett. **91**, 237402 (2003).
[36] N. H. Ge, M. T. Zanni, and R. M. Hochstrasser, J. Phys. Chem. A **106**, 962 (2002).
[37] N. Demirdoven, M. Khalil, and A. Tokmakoff, Phys. Rev. Lett. **89**, 237401 (2002).
[38] M. T. Zanni, M. C. Asplund, and R. M. Hochstrasser, J. Chem. Phys. **114**, 4579 (2001).
[39] J. D. Hybl, A. A. Ferro, and D. M. Jonas, J. Chem. Phys. **115**, 6606 (2001).
[40] J. D. Hybl, S. M. G. Faeder, A. W. Albrecht, C. A. Tolbert, D. C. Green, and D. M. Jonas, J. Lumin. **87/89**, 126 (2000).
[41] P. Hamm, M. Lim, W. F. DeGrado, and R. M. Hochstrasser, Proc. Natl. Acad. Sci. U.S.A. **96**, 2036 (1999).
[42] S. M. G. Faeder and D. M. Jonas, J. Phys. Chem. A **103**, 10489 (1999).
[43] J. D. Hybl, A. W. Albrecht, S. M. G. Faeder, and D. M. Jonas, Chem. Phys. Lett. **297**, 307 (1998).
[44] L. Lepetit and M. Joffre, Opt. Lett. **21**, 564 (1996).
[45] A. Tokmakoff and M. D. Fayer, J. Chem. Phys. **103**, 2810 (1995).
[46] V. M. Kenkre, A. Tokmakoff, and M. D. Fayer, J. Chem. Phys. **101**, 10618 (1994).
[47] S. D. McGrane, R. J. Scharff, and J. Barber, J. Opt. Soc. Am. B **23**, 2217 (2006).
[48] M. Khalil, N. Demirdoven, and A. Tokmakoff, J. Phys. Chem. A **107**, 5258 (2003).
[49] D. M. Jonas, Annu. Rev. Phys. Chem. **54**, 425 (2003).
[50] J. C. Wright, Int. Rev. Phys. Chem. **21**, 185 (2002).
[51] N. H. Ge and R. M. Hochstrasser, PhysChemComm **5**, 17 (2002).
[52] S. Mukamel, *Principles of Nonlinear Optical Spectroscopy* (Oxford University Press, New York, 1995).
[53] N. Demirdoven, M. Khalil, O. Golonzka, and A. Tokmakoff, J. Phys. Chem. A **105**, 8025 (2001).
[54] G. Lupke, N. H. Tolk, and L. C. Feldman, J. Appl. Phys. **93**, 2317 (2003).
[55] C. Manfredotti, F. Fizzotti, M. Boero, P. Pastorino, P. Polesello, and E. Vittone, Phys. Rev. B **50**, 18046 (1994).